TRENDS IN SCIENCES 2026; 23(2): 11289
https://doi.org/10.48048/tis.2026.11289 RESEARCH ARTICLE

Revealing the Anti-Breast Cancer Potential of Essential Oil from Jungga Orange Peel (*Citrus jambhiri*): Network Pharmacology and *In Vitro* Studies

Fauzul Husna[1], Poppy Anjelisa Zaitun Hasibuan[1,*], Panal Sitorus[2], Denny Satria[2], Syukur Berkat Waruwu[3], Ema Damayanti[4] and Najihah Binti Hashim[5]

[1]*Department of Pharmacology, Faculty of Pharmacy, Universitas Sumatera Utara, Medan 20155, Indonesia*
[2]*Department of Pharmaceutical Biology, Universitas Sumatera Utara, Medan 20155, Indonesia*
[3]*Faculty of Pharmacy and Health Sciences, Universitas Sari Mutiara Indonesia, Medan 20123, Indonesia*
[4]*Research Center for Food Technology and Processing, National Research and Innovation Agency, Yogyakarta 55861, Indonesia*
[5]*Department of Pharmaceutical Chemistry, Faculty of Pharmacy, Universiti Malaya, Kuala Lumpur 50603, Malaysia*

([*]Corresponding author's e-mail: poppyanjelisa@usu.ac.id)

Received: 16 July 2025, Revised: 23 July 2025, Accepted: 30 July 2025, Published: 1 November 2025

Abstract

Essential oils from citrus peels, particularly *Citrus jambhiri* (Jungga orange), are gaining attention for their anticancer properties due to the presence of monoterpenes like D-limonene, γ-terpinene, and β-pinene. Despite its bioactive profile, CEO remains underexplored. This study evaluates the anticancer activity of *Citrus jambhiri* essential oil (CEO) using GC-MS profiling, network pharmacology, and *in vitro* testing on T47D breast cancer cells. CEO was extracted via microwave-assisted hydrodistillation, and its constituents were identified through GC-MS. Target genes were predicted using SwissTargetPrediction, PubChem, and CTD, while breast cancer-associated genes were retrieved from GeneCards and Open Targets. Protein-protein interaction and hub genes were analysed using STRING and Cytoscape, with pathway enrichment assessed using DAVID and ShinyGO. Bioactivity was evaluated via MTT, Annexin V/PI, cell cycle, ROS, and protein expression assays targeting PI3K/Akt/mTOR and BTK pathways. CEO was found to be rich in hydrocarbon monoterpenes, mainly D-limonene (35.68%), γ-terpinene (16.14%), and β-pinene (11.84%). Network pharmacology revealed 406 overlapping targets enriched in PI3K/Akt/mTOR and BTK signalling. Key hub genes included AKT1, EGFR, BTK, and TP53. CEO exhibited moderate cytotoxicity (IC_{50} = 68 µg/mL) with high selectivity (SI = 4.67) compared to doxorubicin. Cell-cycle analysis showed S-phase arrest and sub-G1 elevation, while Annexin V/PI confirmed apoptotic activity with minimal necrosis. ROS levels remained unchanged, and CEO significantly downregulated PI3K, mTOR, and BTK, sparing Akt. CEO demonstrates selective anticancer activity through S-phase arrest, non-oxidative apoptosis, and inhibition of PI3K/mTOR-BTK signalling in T47D cells, suggesting its promise as an adjuvant in breast cancer therapy alongside conventional drugs such as doxorubicin.

Keywords: *Citrus jambhiri*, Essential oil, Breast cancer, T47D cells, Network pharmacology, *In vitro*, Doxorubicin

Introduction

Cancer refers to a pathological condition marked by the unregulated growth and division of cells, which leads to the disruption of their normal architecture and biological roles [1]. Among the many forms of cancer, breast cancer remains one of the most pressing global health challenges. Based on the World Health Organization's 2022 data, breast cancer accounted for approximately 23.8% of all diagnosed cancer cases and contributed to 15.4% of cancer-related mortality among women [2]. These figures underscore the urgent demand for the development of therapeutic options that are not only more effective but also less harmful. Conventional

breast cancer treatments include surgery, chemotherapy, radiation therapy, hormonal therapy, and targeted molecular approaches [3]. Although these modalities are clinically proven, they often produce significant adverse effects such as systemic toxicity, immune suppression, and organ damage, which severely compromise patient quality of life [4]. Furthermore, therapeutic resistance, treatment failure, and high costs remain substantial challenges that limit the success of standard therapies [5].

In recent years, plant-derived compounds have gained increasing attention as complementary or alternative therapeutic agents for cancer. Among them, essential oils (EOs) extracted from aromatic and medicinal plants possess a broad range of pharmacological activities including antioxidant, anti-inflammatory, antimicrobial, and notably, anticancer properties [6,7]. These volatile compounds are rich in bioactive terpenoids, especially monoterpenes, which have shown promising effects on cancer cell proliferation, apoptosis, and signalling regulation. Studies have demonstrated that certain monoterpenes such as limonene, α-pinene, and β-elemene can modulate key pathways such as PI3K/Akt/mTOR, Bcl-2/p53, and cell cycle checkpoints, contributing to tumor growth inhibition [8-10].

Citrus jambhiri (Jungga orange), a lesser-known citrus species found in Southeast Asia, has traditionally been used in ethnomedicine but remains underexplored in modern pharmacological research. The essential oil derived from its peel is dominated by monoterpenes especially limonene along with other minor constituents such as 1.4-cyclohexadiene, β-pinene, and β-ocimene [11]. To date, the extraction of essential oils from *Citrus jambhiri* fruit peels reported in various studies has predominantly relied on conventional hydrodistillation methods. This approach is time-consuming, energy-intensive, and relatively inefficient, often leading to the degradation of heat-sensitive bioactive compounds.

In this study, Microwave-Assisted Extraction (MAE) was employed due to its established advantages over conventional extraction techniques. MAE facilitates rapid and uniform heating of plant materials and solvents using microwave energy, resulting in enhanced mass transfer and cell wall disruption. This leads to increased extraction efficiency, shorter processing time, and reduced thermal degradation of bioactive compounds [12-15]. To ensure the chemical integrity and composition of the extracted oil, the volatile constituents were subsequently identified and characterized using Gas Chromatography-Mass Spectrometry (GC-MS) [16]. While the antibacterial properties of *Citrus jambhiri* essential oil have been reported previously, scientific evidence regarding its cytotoxic or anticancer effects, particularly against breast cancer cells, remains scarce.

This study not only introduced an improved extraction method but also advanced the field by investigating the anticancer potential of the *Citrus jambhiri* essential oil. This systematic approach, combining high-efficiency extraction (MAE), compound identification (GC-MS), computational target prediction (network pharmacology), and *in vitro* validation, provides a robust foundation for the therapeutic evaluation of *Citrus jambhiri* essential oil as a promising adjuvant candidate in the development of breast cancer therapy. T47D breast cancer cells were chosen as an *in vitro* model due to their well-characterised hormonal receptor profile (ER+, PR+) and high PI3K/Akt/mTOR signalling activity, including the involvement of non-canonical axes such as BTK, which correspond to the molecular targets investigated in this study. Compared with other commonly used cell lines such as MCF-7 or triple-negative models such as MDA-MB-231, T47D cells provide a more appropriate context to evaluate the mechanism of action of CEO, especially in hormone-sensitive breast cancer [17-19].

Materials and methods

CEO extraction

Essential oil from *Citrus jambhiri* peel (CEO) was obtained through Microwave-Assisted Extraction (MAE). In this process, 50 g of dried and finely ground peel material were introduced into a 1-liter round-bottom flask containing 300 mL of distilled water. The extraction was carried out by heating the mixture in a microwave oven at a controlled temperature of 90 ± 5 °C for 30 min. To enhance the yield, the distillation was conducted in 3 successive cycles. The oil layer was then separated from the aqueous portion using a separatory funnel and transferred into an amber glass vial, where it was stored at 4 °C until further examination [8].

Determination of the chemical composition of CEO

The chemical profile of the essential oil was determined using gas chromatography–mass spectrometry (GC-MS) equipped with a DB-5MS capillary column (30 m×0.25 mm internal diameter, 0.25 μm film thickness). Helium served as the carrier gas, maintained at a constant flow rate of 1.0 mL/min. The oven temperature program began at 40 °C (held for 1 min), followed by a gradual increase to 280 °C at a rate of 3 °C/min, and was held at the maximum temperature for 5 min. The sample was introduced using a split injection mode at a ratio of 100:1. Electron impact (EI) ionization was employed at 70 eV, with the ion source maintained at 200 °C and system pressure set to 50 kPa. Compound identification was performed by matching retention indices and mass spectra against entries in the NIST and Wiley spectral libraries [20].

Target gene prediction

To identify potential gene targets of the bioactive compounds present in CEO, 3 publicly available databases were utilized: PubChem (https://pubchem.ncbi.nlm.nih.gov/), the Comparative Toxicogenomics Database (CTD; http://ctdbase.org/), and Swiss Target Prediction (http://www.swisstargetprediction.ch/). The chemical structures of each CEO component were retrieved from PubChem using compound ID (CID) in canonical SMILES format. These SMILES notations were then submitted to CTD and SwissTargetPrediction to predict relevant molecular targets. To identify genes associated with breast cancer, two disease-related databases - GeneCards (https://www.genecards.org/) and Open Targets (https://www.opentargets.org/) were queried using the keyword "breast cancer." The predicted targets of CEO were then compared with breast cancer-associated genes, and overlapping genes were considered potential therapeutic targets [21,22].

Protein-protein interaction (PPI) network analysis

A protein-protein interaction (PPI) network was constructed to explore how the predicted targets of CEO may interact with genes relevant to breast cancer. Overlapping gene targets were uploaded to the STRING database (https://string-db.org/), with *Homo sapiens* specified as the reference organism, to build a network illustrating potential functional relationships. The generated interaction map was then visualized and analyzed using Cytoscape software (version 3.10.3). To determine the most influential genes in the network, topological properties such as degree centrality, betweenness centrality, and closeness centrality were assessed through the CytoHubba plugin [23,24].

Functional annotation and pathway analysis of hub genes

To assess the functional significance of hub genes implicated in the anticancer effects of CEO, enrichment and annotation analyses were carried out. Gene Ontology (GO) terms - covering biological processes (BP), molecular functions (MF), and cellular components (CC) - along with Kyoto Encyclopedia of Genes and Genomes (KEGG) pathways, were examined using the DAVID database (https://david.ncifcrf.gov/). For enhanced graphical interpretation, GO enrichment was also performed via ShinyGO version 0.77, applying a false discovery rate (FDR) cutoff of < 0.05. The ten most significantly enriched GO terms from each category were selected for detailed analysis. Furthermore, the SRplot platform (https://www.bioinformatics.com.cn/) was employed to visualize the thirty top-ranking KEGG pathways, offering insight into the potential molecular mechanisms regulated by CEO [25].

MTT assay

The cytotoxic potential of CEO was assessed through an MTT colorimetric assay. T47D breast cancer cells were seeded into 96-well plates at a suitable density and incubated at 37 °C for 24 h in a humidified environment containing 5% CO_2 to promote cell adherence. After incubation, the cells were exposed to serial dilutions of CEO (250, 125, 62.5, 31.25 and 15.625 μg/mL). Doxorubicin, used as a positive control, was applied at concentrations of 1.25, 0.625, 0.3125, 0.156 and 0.078 μg/mL. Following 48 h of treatment, 200 μL of culture medium supplemented with MTT reagent (0.5 mg/mL) was added to each well and incubated for an additional 3 h. After discarding the medium, the formazan crystals formed were solubilized in 100 μL of DMSO. Absorbance readings were taken at 595 nm using a microplate reader. Cell viability was

expressed as a percentage relative to the untreated control, and IC_{50} values were derived from nonlinear regression analysis of the dose-response curves. All assays were conducted in triplicate across 3 independent experiments [17,26].

Cell cycle analysis

Flow cytometry was employed to assess cell cycle progression in T47D breast cancer cells following treatment with CEO. Cells were cultured in 6-well plates and maintained at 37 °C in a humidified incubator with 5% CO_2 for 24 h to ensure attachment. Afterward, the culture medium was replaced with fresh medium containing CEO, and incubation was continued for another 48 h under identical conditions. Post-treatment, both adherent and suspended cells were collected via trypsinization, rinsed twice with cold phosphate-buffered saline (PBS), and fixed overnight in 70% ethanol at –20 °C. The following day, the fixed cells were centrifuged, washed, and treated with RNase A (100 µg/mL) and propidium iodide (PI) (50 µg/mL) for 30 min at room temperature in the absence of light. DNA content was then analyzed using flow cytometry, and the proportions of cells in G0/G1, S, and G2/M phases were quantified using dedicated cell cycle analysis software [27,28].

Apoptosis analysis

Apoptosis in T47D cells following treatment with CEO was examined using dual staining with Annexin V-FITC and propidium iodide (PI), followed by flow cytometric analysis. Cells were seeded into 6-well plates and incubated at 37 °C in a humidified atmosphere with 5% CO_2 for 24 h to allow attachment. After 48 h of CEO exposure, both adherent and floating cells were harvested via trypsinization, rinsed twice with cold phosphate-buffered saline (PBS), and centrifuged. Cell pellets were then resuspended in 100 µL of binding buffer containing Annexin V-FITC and PI, following the staining protocol provided by the manufacturer. The cell suspension was incubated in the dark at room temperature for 15 min. Following this, 400 µL of binding buffer was added, and the samples were immediately analyzed using a FACScan flow cytometer (Becton Dickinson, USA). The proportions of viable, early apoptotic, late apoptotic, and necrotic cells were determined based on quadrant analysis of dual-parameter dot plots [29,30].

PI3K, Akt, and mTOR protein expression analysis

T47D cells were cultured in 6-well plates and incubated for 48 h at 37 °C under a 5% CO_2 atmosphere. After exposure to either CEO or control medium for 48 h, both adherent and suspended cells were collected using 0.025% trypsin, rinsed twice with phosphate-buffered saline (PBS), and subjected to centrifugation. The resulting pellets were incubated with monoclonal antibodies targeting PI3K, Akt, or mTOR for 10 min at 37 °C in the absence of light. Following the staining procedure, the cells were washed again and analyzed using a FACScan flow cytometer to assess the expression levels of the respective proteins [31-33].

BTK expression analysis

Intracellular flow cytometry was employed to assess the expression of BTK, a signalling component associated with the PI3K/Akt/mTOR pathway. T47D cells were seeded in 6-well plates and exposed to either CEO or control medium for 24 h under standard incubation conditions (37 °C, 5% CO_2). Post-treatment, cells were collected, washed twice with cold PBS, and fixed in 4% paraformaldehyde for 15 min at room temperature. Following fixation, cells were permeabilized using a commercial buffer and incubated with fluorochrome-labeled anti-BTK monoclonal antibodies for 30 to 60 min at 4 °C in the dark. Isotype-matched antibodies served as negative controls. After a final washing step, cells were resuspended in PBS and subjected to flow cytometric analysis to quantify intracellular BTK expression based on fluorescence intensity [34].

Measurement of ROS

Intracellular reactive oxygen species (ROS) levels were assessed using the cell-permeable fluorescent probe CM-H_2DCFDA (5-(and-6)-chloromethyl-2',7'-dichlorodihydrofluorescein diacetate), which becomes fluorescent upon oxidation by ROS. T47D cells were seeded and treated with CEO or control medium for 24 h at 37 °C in a humidified incubator containing 5% CO_2. After treatment, cells were rinsed twice with PBS and incubated in a serum-free medium containing CM-

H_2DCFDA (5 - 10 μM) for 30 min at 37 °C in the dark. Following incubation, excess dye was removed by washing with PBS. The resulting fluorescence of the oxidized product, DCF (2',7'-dichlorofluorescein), was measured using a flow cytometer with excitation at 492 - 495 nm and emission at 517 - 527 nm. ROS levels were quantified based on mean fluorescence intensity, representing the degree of intracellular oxidative activity [35].

Statistical analysis

All data are expressed as mean ± standard deviation (SD) from 3 independent replicates (n = 3). Statistical analysis was conducted using IBM SPSS Statistics version 26.0. For comparisons between CEO and doxorubicin in terms of IC_{50} and selectivity index (SI), an unpaired *t*-test was applied. One-way analysis of variance (ANOVA) was subsequently employed to assess differences among treatment groups. When a significant effect was detected, Dunnett's post hoc test was used to compare each treatment group to the control. A *p*-value of < 0.001 was considered statistically significant.

Results and discussion

Essential oil yield from *Citrus jambhiri* peel

Essential oil was extracted from dried *Citrus jambhiri* peel using the Microwave-Assisted Extraction (MAE) method. Three separate batches were processed, each with approximately 50 grams of dried, powdered peel. The volumes of essential oil obtained were 6.0, 7.5 and 7.0 mL, corresponding to yields of 11.98, 14.99, and 13.99 %(v/w), respectively. The total yield from all 3 batches was 20.5 mL from 150.11 g of dried material, with an average essential oil content of 13.65 ± 1.53 %(v/w).

This yield is significantly higher than those typically reported for conventional hydrodistillation methods, which range from 0.72% to a maximum of 4.0% [36,37]. The enhanced yield may be attributed to the MAE mechanism, which uses rapid volumetric heating via microwave energy to accelerate cell wall rupture and improve the diffusion of volatile compounds from plant tissues. MAE minimizes thermal degradation of heat-sensitive terpenoids - particularly monoterpenes such as limonene and β-pinene - due to its short extraction time (30 min at 90 ± 5 °C), allowing better preservation of active compound profiles compared to conventional methods [36,38]. Additionally, water used as the extraction medium, acts as a microwave-absorbing matrix, promoting the efficient release of bioactive compounds without the need for organic solvents [39].

Chemical profiling of *Citrus jambhiri* peel essential oil via GC-MS analysis

GC-MS analysis of CEO identified 60 volatile constituents (**Figure 1**). Among these, the 20 most abundant compounds were selected and are presented in the chromatographic profile (**Table 1**), collectively representing 93.43% of the total peak area. This composition reflects the primary chemical profile of the oil. CEO was predominantly composed of monoterpene hydrocarbons, with D-limonene (35.68%) as the most abundant compound, followed by γ-terpinene (16.14%), β-pinene (11.84%), α-pinene (4.75%), and β-myrcene (3.83%).

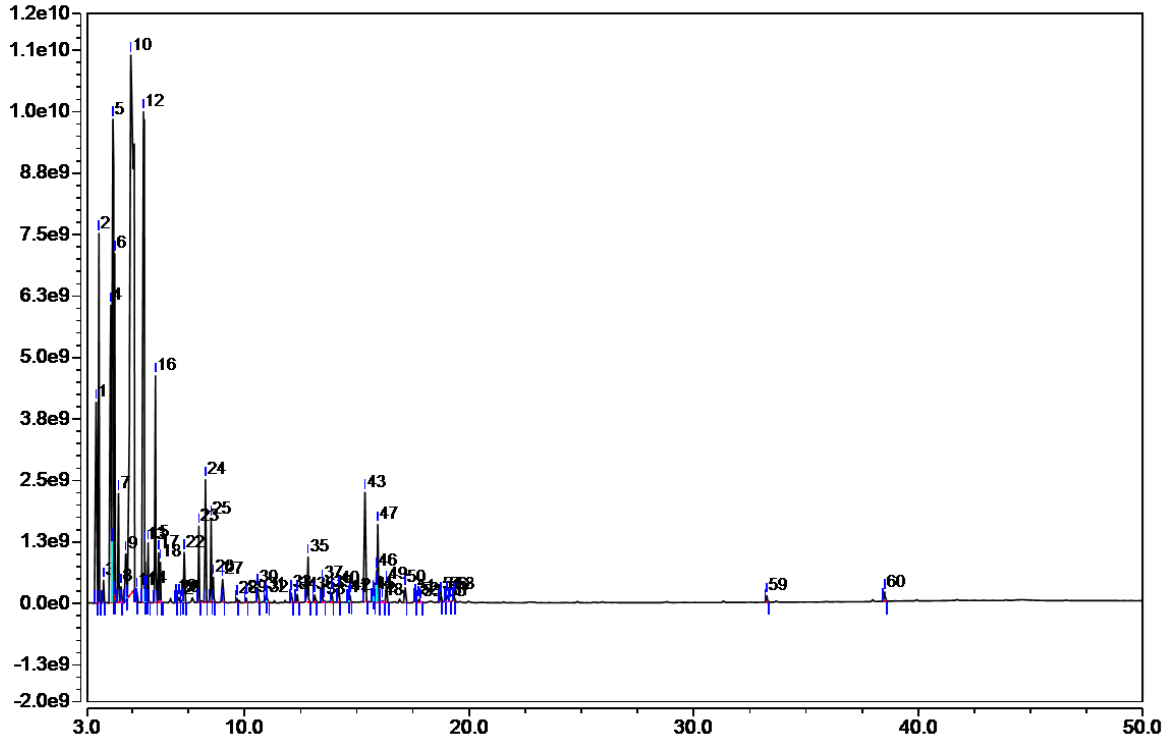

Figure 1 GC-MS chromatogram of CEO showing the identified volatile constituents.

The classification of all identified compounds is summarized in **Table 2**. Monoterpene hydrocarbons were the dominant chemical class, accounting for 73.57% of the total peak area, followed by cyclic hydrocarbons (12.85%) and oxygenated monoterpenes (5.91%). Other classes, such as aliphatic aldehydes, sesquiterpene hydrocarbons, fatty acid esters, and oxygenated hydrocarbons, each contributed less than 4%. A small fraction (0.81%) remained unclassified due to limited structural information. GC-MS profiling confirmed that CEO is primarily composed of monoterpene hydrocarbons, which account for over 70% of the detected compounds. The major constituents - D-limonene, γ-terpinene, β-pinene, α-pinene, and β-myrcene - form a characteristic chemical fingerprint typical of essential oils from the *Citrus* genus [40,41]. The predominance of D-limonene is consistent with findings from other *Citrus* species such as *C. sinensis* and *C. reticulata*, which also exhibit high limonene content and have been reported to possess cytotoxic activity against breast, lung, and colon cancer cell lines [42,43].

Table 1 The 20 most abundant compounds identified in CEO by GC-MS, representing 93.43% of the total peak area.

Rank	Compound name	Retention time	Area (%)	Class
1	D-limonene	4.94	35.68	Hydrocarbon monoterpenes
2	γ-Terpinene	5.50	16.14	Hydrocarbon monoterpenes
3	β-Pinene	4.14	11.84	Hydrocarbon monoterpenes
4	Bicyclo[3.1.0]hexane, 4-methylene-1-(1-methylethyl)-	4.05	6.20	Cyclic hydrocarbons
5	α-pinene	3.52	4.75	Hydrocarbon monoterpenes
6	β-Myrcene	4.22	3.83	Hydrocarbon monoterpenes
7	Cyclohexene, 3-methyl-6-(1-methylethylidene)-	6.03	2.55	Cyclic hydrocarbons

Rank	Compound name	Retention time	Area (%)	Class
8	Bicyclo[3.1.0]hex-2-ene, 4-methyl-1-(1-methylethyl)-	3.39	2.11	Cyclic hydrocarbons
9	α-Terpineol	8.26	1.52	Oxygenated monoterpenes
10	Octanal	4.39	1.29	Aliphatic aldehydes
11	Cyclohexene, 1-methyl-4-(1-methylethylidene)-	4.71	1.20	Cyclic hydrocarbons
12	β-Bisabolene	15.93	1.08	Oxygenated monoterpenes
13	Decanal	8.51	1.02	Aliphatic aldehydes
14	Terpinen-4-ol	7.97	0.93	Oxygenated monoterpenes
15	Geranyl acetate	12.83	0.68	Oxygenated monoterpenes
16	Linalool	6.17	0.58	Oxygenated monoterpenes
17	6-Octenal, 3,7-dimethyl-, (S)-	7.31	0.57	Aliphatic aldehydes
18	2-Furanmethanol, 5-ethenyltetrahydro-α,α,5-trimethyl-, cis-	5.71	0.54	Oxygenated monoterpenes
19	Cyclopropane, pentyl-	5.57	0.49	Aliphatic hydrocarbons
20	Nonanal	6.25	0.42	Aliphatic aldehydes

Table 2 Classification of volatile compounds identified in CEO based on chemical structure and functional groups.

Rank	Compound class	Number of compounds	Total area (%)
1	Monoterpene hydrocarbon	9	73.57
2	Cyclic hydrocarbon (non-terpene)	7	12.85
3	Oxygenated monoterpene	20	5.91
4	Aliphatic aldehyde	6	3.67
5	Unclassified	7	0.81
6	Sesquiterpene hydrocarbon	5	0.65
7	Fatty acid ester	3	0.53
8	Oxygenated hydrocarbon	1	0.29

Integration of molecular targets between *Citrus jambhiri* essential oil compounds and breast cancer-associated genes

To enable a network pharmacology analysis, the 10 most abundant constituents of CEO were selected based on their relative concentrations determined by GC–MS. These compounds not only represent the core chemical profile of CEO but also possess known pharmacological properties, particularly within cancer-related signalling pathways. This focused selection facilitates a biologically relevant and interpretable computational analysis. A network pharmacology approach was employed to explore the potential interactions between these bioactive CEO constituents and molecular targets associated with breast cancer. Target prediction for the selected CEO compounds was conducted using the Comparative Toxicogenomics Database (CTD) and SwissTargetPrediction, resulting in 451 unique compound-associated genes.

In parallel, breast cancer-related genes were retrieved from 2 major databases: GeneCards (17.622 genes) and Open Targets (11.854 genes). An

intersection of these datasets revealed 9.847 overlapping genes (50.2%) (**Figure 2(a)**), reflecting the complementary nature of the 2 platforms. GeneCards integrates diverse genomic and proteomic data, while Open Targets focuses on clinically and experimentally validated therapeutic targets. These 9.847 overlapping genes were selected as the breast cancer gene set for further analysis. A comparison with the 451 predicted CEO compound targets identified 406 shared genes (4.1%) (**Figure 2(b)**). Although this represents a modest percentage, the absolute number of overlapping genes is substantial, providing a robust basis for downstream network construction and functional enrichment analysis. This intersection suggests that CEO bioactive components may influence critical molecular mechanisms involved in breast cancer pathogenesis. The high proportion (over 90%) of CEO-predicted targets found within the breast cancer gene pool underscores the relevance of CEO compounds to this disease context. Such findings are in line with current network pharmacology studies that leverage systems biology to identify natural product-based therapeutic candidates [44,45]. In addition, the overlapping target profiles of key CEO constituents such as D-limonene, γ-terpinene, and β-pinene suggest the possibility of pharmacological synergism among these compounds. Although direct evidence of compound-to-compound interactions remains limited, one study has reported a synergistic effect between α- and β-pinene in enhancing cancer cell cytotoxicity, including increased apoptosis and more effective inhibition of proliferation than individual components [46]. This supports the notion that the anticancer activity of CEO arises not from a single constituent, but from a multi-component synergy that collectively enhances its cytotoxic effects.

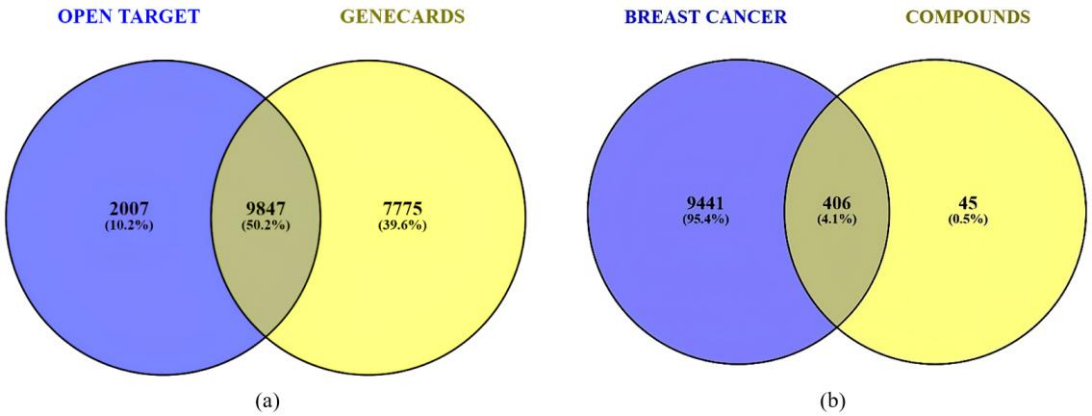

Figure 2 (a) Overlapping breast cancer-associated genes from GeneCards (17.622 genes) and Open Targets (11.854 genes), resulting in 9.847 shared genes. (b) Venn diagram showing the intersection of 451 predicted CEO compound targets with 9.847 breast cancer-related genes, identifying 406 common targets.

Protein-protein interaction (PPI) network and Hub Gene analysis

To identify key molecular targets potentially modulated by CEO in breast cancer, a protein-protein interaction (PPI) network was constructed from 406 overlapping genes shared between CEO-related targets and breast cancer-associated genes. The network was analyzed using the STRING database and visualized with Cytoscape software. Hub gene analysis was conducted using the CytoHubba plugin, employing 3 topological centrality metrics: Degree, betweenness, and closeness. These metrics reflect node connectivity, control over information flow, and proximity to other nodes, respectively [47]. Based on degree centrality, the top 3 hub genes were TP53, AKT1, and MYC, indicating their high levels of interaction with other genes within the network (**Figure 3(a)**). For betweenness centrality, TP53, AKT1, and ALB emerged as key intermediaries (**Figure 3(b)**), while closeness centrality ranked TP53, AKT1, and ESR1 as the most centrally located nodes (**Figure 3(c)**). Across all 3 analyses, TP53 consistently ranked highest, highlighting its central regulatory role in multiple cancer-related signalling pathways [48]. Despite its prominent network position, TP53 was excluded from experimental validation because the T47D cell line used

in the *in vitro* study harbors a loss-of-function mutation in this gene. As a result, PI3K, Akt, and mTOR were selected for validation instead, as these targets are functionally intact in the model system and aligned with the computational predictions [49]. AKT1 served as a bridge between network-based findings and experimental validation, reinforcing the biological relevance of the selected pathway. Node color intensity in **Figure 3** represents centrality scores, with redder nodes indicating greater influence in the network and the top 10 genes ranked by each centrality measure are presented.

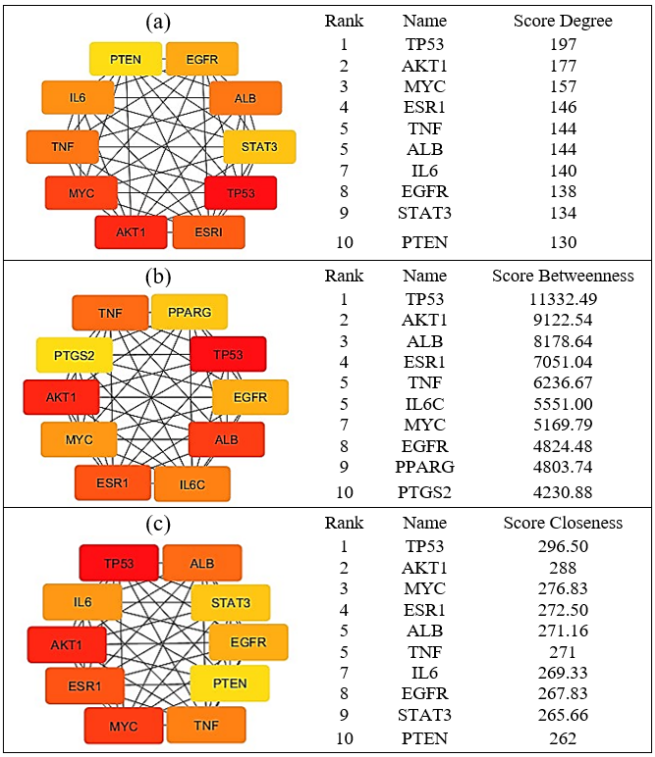

Rank	Name	Score Degree
1	TP53	197
2	AKT1	177
3	MYC	157
4	ESR1	146
5	TNF	144
5	ALB	144
7	IL6	140
8	EGFR	138
9	STAT3	134
10	PTEN	130

Rank	Name	Score Betweenness
1	TP53	11332.49
2	AKT1	9122.54
3	ALB	8178.64
4	ESR1	7051.04
5	TNF	6236.67
5	IL6C	5551.00
7	MYC	5169.79
8	EGFR	4824.48
9	PPARG	4803.74
10	PTGS2	4230.88

Rank	Name	Score Closeness
1	TP53	296.50
2	AKT1	288
3	MYC	276.83
4	ESR1	272.50
5	ALB	271.16
5	TNF	271
7	IL6	269.33
8	EGFR	267.83
9	STAT3	265.66
10	PTEN	262

Figure 3 Hub gene analysis of the CEO–breast cancer PPI network using Cytoscape (CytoHubba). (a) Degree centrality, (b) Betweenness centrality, and (c) Closeness centrality. Red nodes indicate genes with higher centrality scores. The top 10 genes and their corresponding scores for each metric are shown in the accompanying tables.

Functional annotation and pathway analysis of CEO Hub Genes

Gene Ontology (GO) and Kyoto Encyclopedia of Genes and Genomes (KEGG) enrichment analyses were conducted to explore the molecular mechanisms potentially underlying the anti-cancer activity of CEO. The results indicated that the hub genes identified from the PPI network are predominantly associated with transcriptional regulation, xenobiotic response, and suppression of cell proliferation signals. In the Biological Process (BP) category, "response to xenobiotic stimulus" was the most significantly enriched term, followed by "positive regulation of transcription by RNA polymerase II." For the Cellular Component (CC) category, the top enriched were "nucleus" and "nucleoplasm," indicating a primary nuclear localization of the predicted targets. In the Molecular Function (MF) category, "protein binding" and "nuclear receptor activity" were the most prominent functional annotations (**Figure 4(a)**). KEGG pathway analysis further highlighted significant enrichment in "pathways in cancer" and the "PI3K-Akt signalling pathway," both of which are central to tumorigenesis, cellular proliferation, and survival mechanisms (**Figure 4(b)**). These findings align with the GO results, reinforcing the hypothesis that CEO may influence key oncogenic signalling cascades. To better characterize the roles of these genes, deeper GO annotation and KEGG pathway enrichment analyses were performed. The GO analysis emphasized CEO targets' involvement in processes such as transcriptional activation mediated by RNA polymerase II, regulation of cell proliferation,

and inhibition of apoptotic mechanisms. The predominant cellular components - nucleus, nucleoplasm, and cytosol - further support the relevance of nuclear and cytoplasmic signalling. Functionally, the hub genes demonstrated strong associations with DNA binding, enzyme and receptor interaction, and zinc ion coordination - molecular functions essential for transcriptional regulation and signal transduction [50].

In KEGG analysis, the highest-ranking term was "pathways in cancer," followed by PI3K/Akt, MAPK, BTK, and B-cell receptor signalling pathways. These signalling routes are known to govern cell growth, differentiation, immune modulation, and chemoresistance. Collectively, these results suggest that the monoterpene-rich CEO - particularly through constituents like D-limonene and γ-terpinene - may act as xenobiotic ligands capable of disrupting oncogenic networks by targeting pivotal nodes in the PI3K/Akt/mTOR and BTK pathways [51,52]. The combined GO and KEGG enrichment data provide a comprehensive systems-level perspective on how CEO compounds may modulate cancer-related signalling. This integrative approach strengthens the molecular rationale for further biological validation of CEO in breast cancer models using *in vitro* assays.

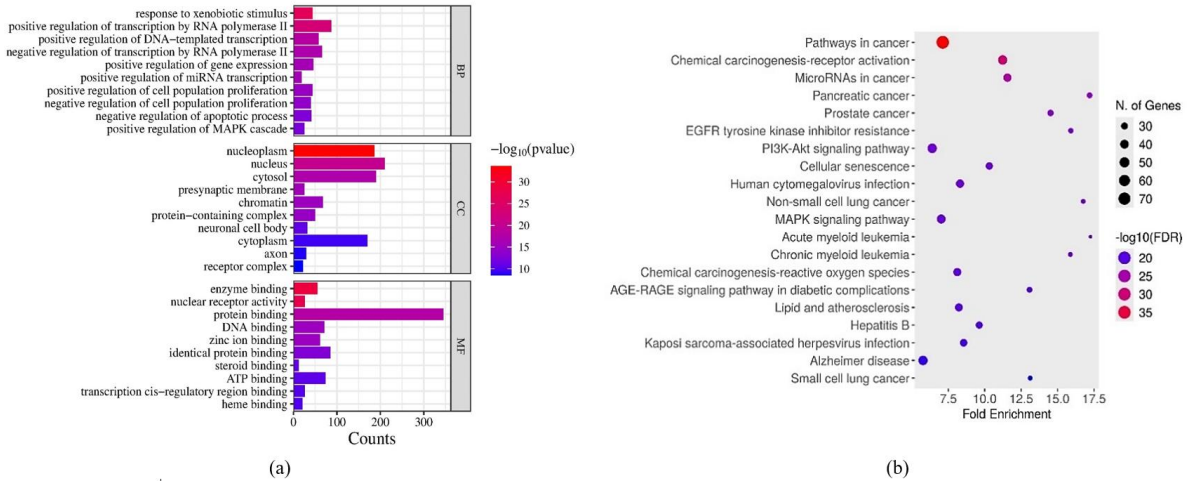

Figure 4 Functional enrichment analysis of CEO hub genes. (a) GO enrichment analysis across 3 domains: Biological Process (BP), Cellular Component (CC), and Molecular Function (MF). (b) KEGG pathway enrichment of hub genes, highlighting cancer-related signalling pathways. The top enriched terms are shown based on *p*-value significance.

Cytotoxicity and selectivity of CEO

The cytotoxic effect of CEO was evaluated using the MTT assay on T47D breast cancer cells. As shown in **Table 3**, CEO exhibited moderate cytotoxicity, with a half-maximal inhibitory concentration (IC_{50}) of 68.49 ± 0.58 µg/mL. In comparison, doxorubicin demonstrated significantly higher potency, with an IC_{50} of 0.096 ± 0.004 µg/mL ($p < 0.001$ vs CEO). However, CEO showed superior selectivity toward cancer cells. Its IC_{50} on normal Vero cells was 319.74 ± 3.30 µg/mL, resulting in a selectivity index (SI) of 4.67 ± 0.04. In contrast, doxorubicin displayed an SI of only 2.13 ± 0.02 ($p < 0.001$ vs CEO), indicating greater cytotoxicity toward non-cancerous cells.

Table 3 IC_{50} values and selectivity indices (SI) of CEO and doxorubicin on T47D breast cancer cells and normal Vero cells.

Sample	IC_{50} T47D (µg/mL)	95% CI	IC_{50} Vero (µg/mL)	95% CI	SI (T47D/Vero)	*p* value
CEO	68.49 ± 0.58	66.9 - 70.1	319.74 ± 3.30	313.5 - 325.8	4.67 ± 0.04	< 0.001
Doxorubicin	0.096 ± 0.004	0.089 - 0.103	0.205 ± 0.002	0.199 - 0.211	2.13 ± 0.02	

These findings suggest that CEO has a more favorable therapeutic window, selectively targeting cancer cells while sparing normal ones. This is further illustrated in **Figure 5**, where CEO induced a concentration-dependent decrease in T47D cell viability, with a marked reduction observed at concentrations above 125 µg/mL. Doxorubicin, on the other hand, produced a sharp decline in viability even at very low concentrations. Consistent with predictions from the network pharmacology analysis, the selective cytotoxicity of CEO may be attributed to its major lipophilic monoterpenes, such as D-limonene, γ-terpinene, and β-pinene. These compounds tend to accumulate in cancer cell membranes due to differences in lipid composition - particularly cholesterol content and lipid saturation - potentially increasing susceptibility to monoterpene-induced cytotoxicity [53-55].

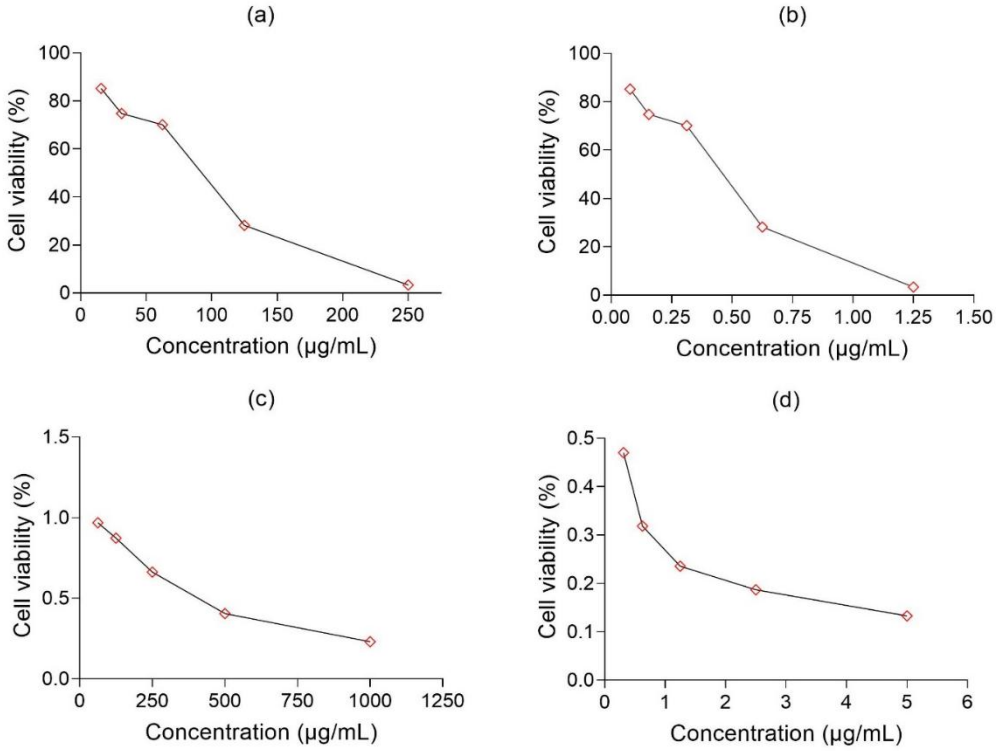

Figure 5 Cell viability of T47D and Vero cells after 48 h of treatment. (a) CEO treatment on T47D cells, (b) Doxorubicin treatment on T47D cells, (c) CEO treatment on Vero cells and (d) Doxorubicin treatment on Vero cells.

Effect on cell cycle and apoptosis

To investigate the mechanism underlying CEO-mediated cytotoxicity, the cell cycle distribution of T47D cells was analyzed by flow cytometry after 48 h of treatment. As shown in **Figure 6(a)**, treatment with CEO at 20 µg/mL slightly increased the Sub-G1 population to 0.43 ± 0.05%, a marker of DNA fragmentation and early apoptosis, while no Sub-G1 population was detected in control cells. In contrast, doxorubicin resulted in a higher Sub-G1 fraction of 0.76 ± 0.05% ($p < 0.001$ vs. CEO), consistent with its known pro-apoptotic effects. Further analysis revealed that CEO treatment caused an increase in the proportion of cells in the S phase and Sub-G1 phase, without significantly affecting the G2/M phase. This profile indicates the presence of replication stress, likely mediated by compounds such as limonene and carveol, which are known to inhibit ribonucleotide reductase, leading to depletion of deoxynucleotide triphosphates (dNTPs) and cell cycle arrest [56]. The accumulation in S phase suggests that CEO may inhibit DNA synthesis and promote programmed cell death.

Quantitative data from cell cycle analysis (**Figure 6(b)**) showed that CEO reduced the G0/G1 population from 62.20 ± 0.26% (control) to 58.20 ± 0.10%, while increasing the S phase fraction from 7.60 ± 0.10% to 11.43 ± 0.05%, indicative of disrupted DNA replication. The G2/M population remained largely unchanged

(30.13 ± 0.15% in control vs. 30.16 ± 0.11% with CEO), suggesting that CEO primarily induces cell cycle arrest before mitosis. In comparison, doxorubicin caused a modest increase in the S phase (8.76 ± 0.05%) and a slight decrease in G2/M (28.90 ± 0.10%) ($p < 0.001$ vs. CEO).

To assess whether S-phase arrest was associated with apoptosis, Annexin V-FITC/PI staining was performed (**Figure 7**). CEO treatment (20 µg/mL) significantly increased both early and late apoptotic populations (6.18% and 14.57%, respectively), while inducing minimal necrosis (3.02%), compared to untreated controls, which largely consisted of viable cells. In contrast, doxorubicin (0.01 µM) markedly reduced cell viability (22.83%) and induced substantial late apoptosis (39.72%) and necrosis (31.88%) ($p < 0.001$ vs. CEO). These findings confirm that CEO selectively induces apoptosis without triggering significant necrosis, suggesting a controlled, non-genotoxic, ROS-independent mechanism of action. This contrasts with doxorubicin, which acts as a DNA intercalator and oxidative stress inducer, resulting in more extensive necrosis. The apoptotic specificity of CEO highlights its potential as a safer adjuvant agent in breast cancer therapy, with reduced risk of off-target tissue damage [57,58].

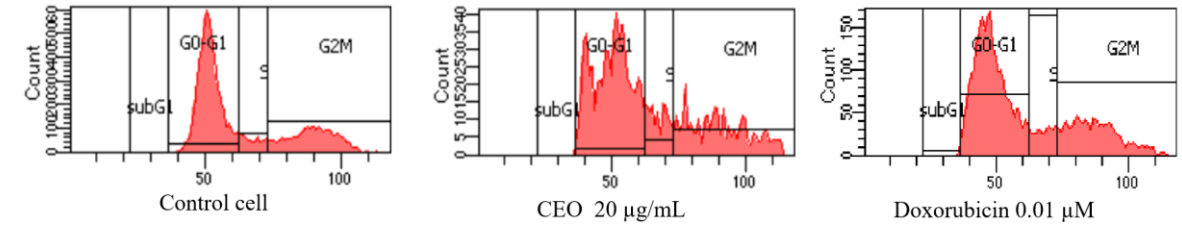

(a)

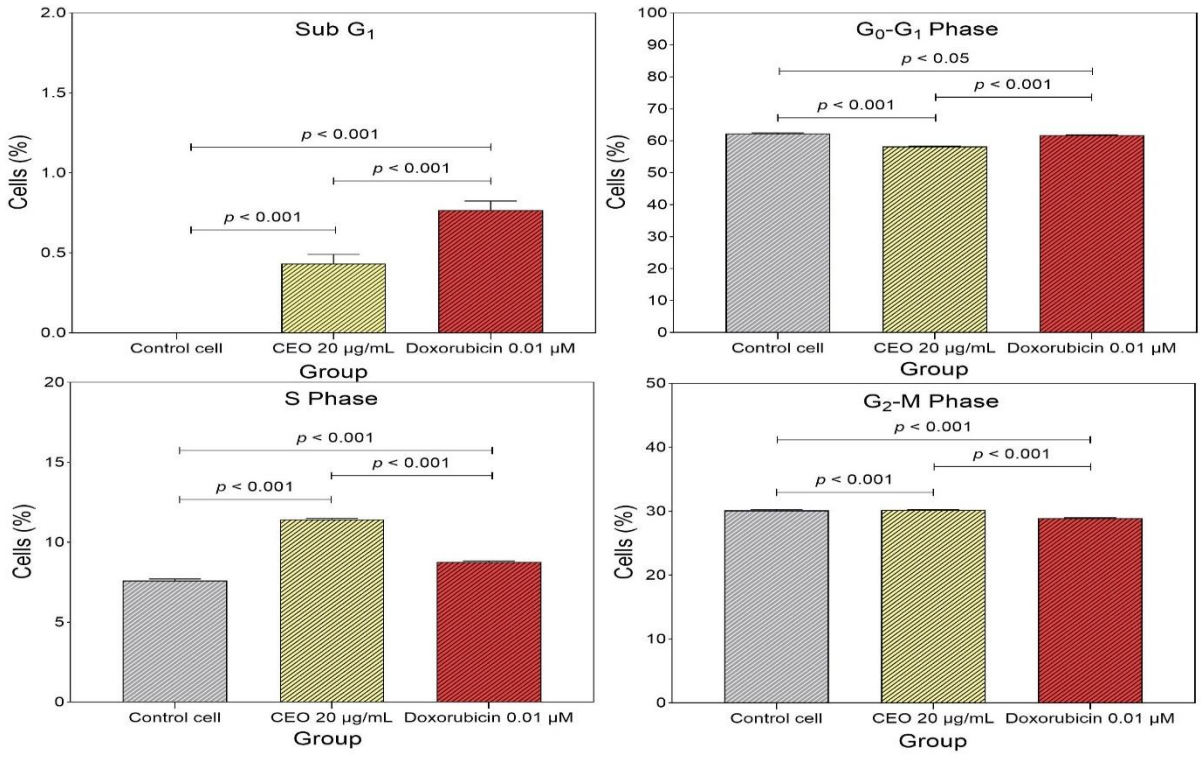

(b)

Figure 6 Cell cycle profiles of T47D cells after 48-hour treatment. (a) Representative PI histograms of cells treated with CEO (20 µg/mL) or doxorubicin (0.01 µM), and control. (b) Quantitative distribution across cell cycle phases (G0/G1, S, G2/M, and Sub-G1). $p < 0.001$ indicates statistical significance.

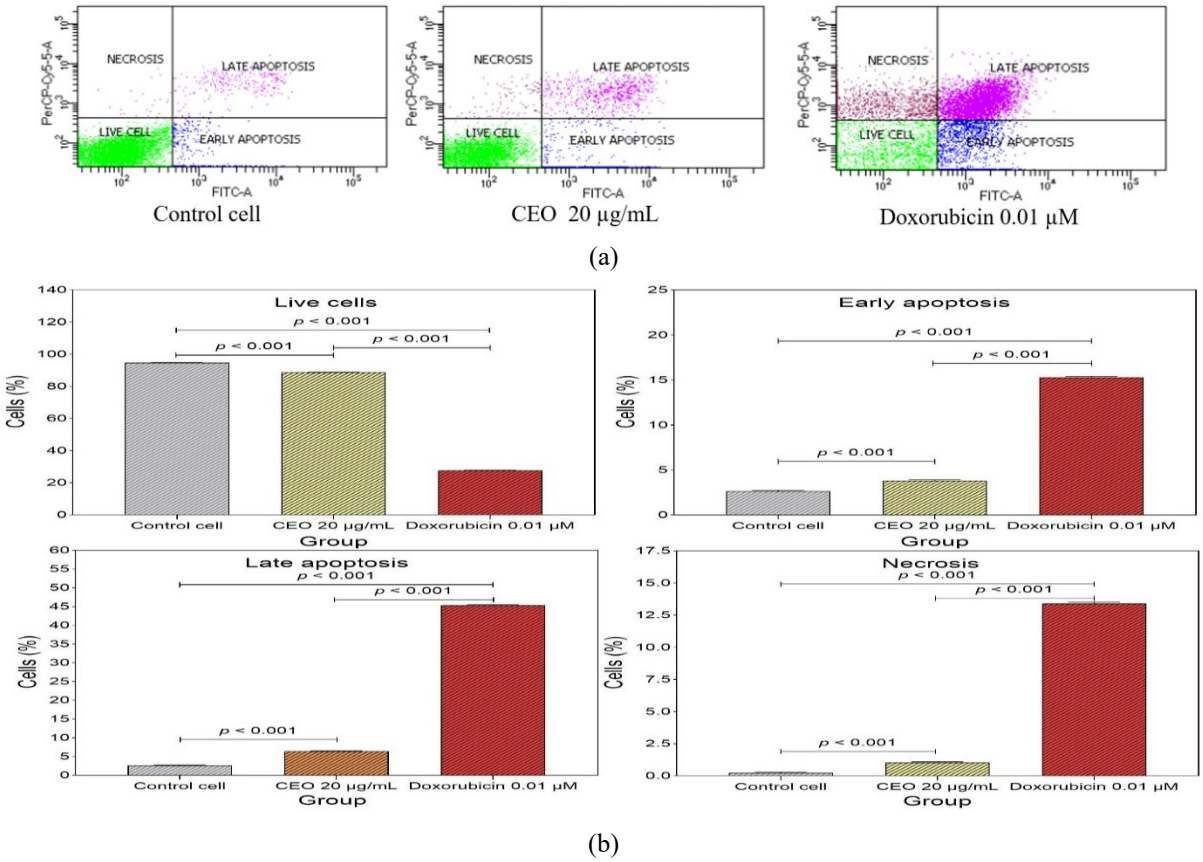

Figure 7 Apoptosis analysis of T47D cells after 48-hour treatment with CEO (20 µg/mL) or doxorubicin (0.01 µM). (a) Representative Annexin V-FITC/PI dot plots showing the distribution of live, early apoptotic, late apoptotic, and necrotic cells. (b) Quantitative comparison of cell populations, expressed as percentages. $p < 0.001$ indicates statistical significance.

Effect on protein expression

Protein expression analysis revealed that CEO downregulated several key survival-related proteins in T47D breast cancer cells (**Figure 8**). Flow cytometry data indicated that treatment with CEO (20 µg/mL) reduced PI3K expression from 92.83% (control) to 81.26% ($p < 0.001$), and mTOR from 90.70% to 70.73% ($p < 0.001$), suggesting inhibition of both upstream and downstream elements of the PI3K/Akt/mTOR signalling pathway. Akt levels were only slightly diminished, from 92.70% to 90.60% ($p < 0.001$), whereas BTK expression decreased from 89.00% to 76.26% ($p < 0.001$), indicating additional modulation of non-canonical survival pathways. As a positive control, doxorubicin (0.01 µM) induced more substantial reductions across all proteins examined: PI3K, Akt, mTOR, and BTK levels decreased to 58.86%, 75.37%, 67.50%, and 51.10%, respectively ($p < 0.001$ vs. control; $p < 0.001$ vs. CEO).

Quantitatively, CEO treatment led to a 12% reduction in PI3K, 20% in mTOR, and 13% in BTK, with minimal effect on Akt (only 2%). This selective inhibition suggests a targeted suppression of the PI3K/mTOR axis and BTK, while sparing Akt - an essential kinase involved in metabolic regulation in normal cells. Such selectivity may help avoid adverse metabolic effects typically observed with broad-spectrum Akt inhibitors [59,60]. Notably, this dual inhibition was achieved by a natural mixture of CEO compounds, potentially eliminating the need for multi-drug regimens.

Integration of GC-MS profiles, *in silico* predictions, and *in vitro* validation provides a mechanistic framework for CEO's anticancer activity. Major CEO constituents - D-limonene, γ-terpinene, and β-pinene - likely bind to the catalytic sites of PI3K, mTOR, and BTK, thereby disrupting key proliferative and survival signalling cascades in cancer cells. This action contributes to S-phase arrest, likely through

dNTP depletion caused by ribonucleotide reductase inhibition, followed by non-oxidative, caspase-dependent apoptosis [61]. Each major CEO compound plays a distinct role in regulating cancer-associated signalling pathways, particularly the PI3K/Akt/mTOR-BTK axis. D-limonene is reported to inhibit PI3K by directly targeting the catalytic domain of the p110α subunit, leading to suppression of Akt activation via PIP_3 inhibition. γ-Terpinene stabilizes the tumor suppressor protein p53 and attenuates mTORC1 activity. Additionally, α- and β-pinene have demonstrated BTK-inhibitory activity, interfering with non-canonical pathways relevant to aggressive breast cancer phenotypes [62,63].

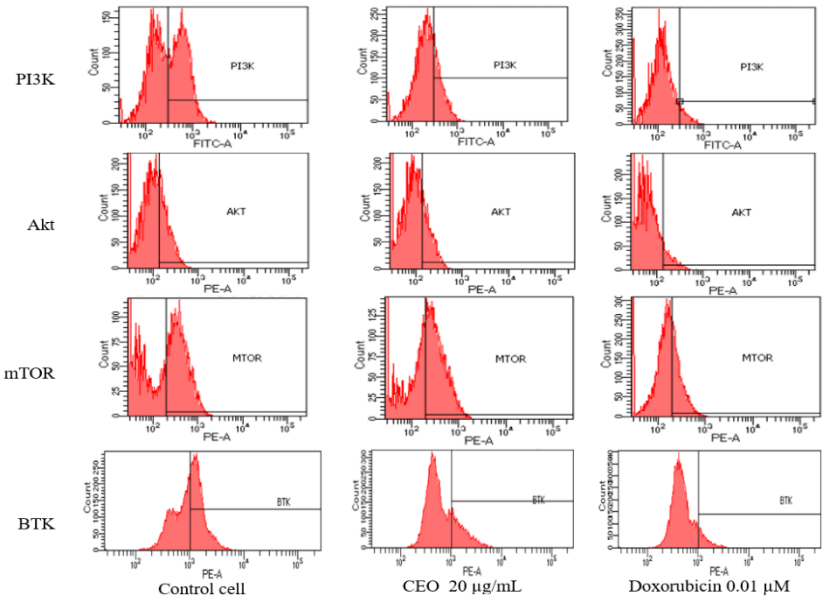

(a)

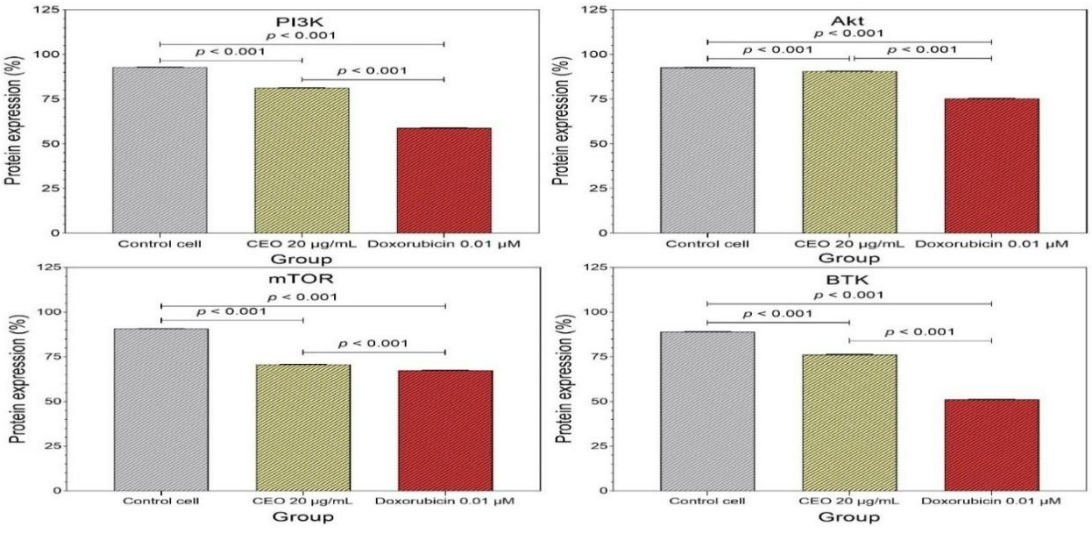

(b)

Figure 8 Protein expression analysis of PI3K, Akt, mTOR, and BTK in T47D cells after 48-hour treatment with CEO (20 µg/mL) or doxorubicin (0.01 µM). (a) Representative flow cytometry histograms showing fluorescence intensity for each target protein. (b) Quantification of relative protein expression levels in treated versus control groups. $p < 0.001$ indicates statistical significance.

ROS analysis

Flow cytometry analysis of intracellular ROS levels revealed that CEO at 14 µg/mL did not significantly increase ROS production compared to the untreated control ($p > 0.001$, **Figure 9**). The comparable ROS signal indicates that CEO-induced cytotoxicity is

not primarily mediated through oxidative stress. In contrast, doxorubicin (0.1 µM) elicited a modest reduction in ROS levels relative to both the CEO-treated and control groups ($p < 0.001$), potentially reflecting mitochondrial dysfunction or cellular degradation during late-stage apoptosis. The absence of increased ROS in CEO-treated cells suggests that its cytotoxic mechanism is independent of oxidative pathways, consistent with findings from recent observations that certain essential oils can induce apoptosis through mitochondrial disruption or modulation of the mTOR pathway without increasing ROS [64,65]. In contrast, doxorubicin, known to induce oxidative stress through DNA intercalation and free radical formation, exhibited a paradoxical decrease in ROS levels, possibly due to mitochondrial damage in viable cells, increased mitophagy, or a cellular antioxidant response that regenerates after sustained oxidative stress [66,67].

These findings confirm that CEO induces apoptosis through a ROS-independent mechanism, although the precise molecular pathway remains elucidated. The absence of oxidative stress induction highlights the CEO's suitability as an adjuvant, particularly when combined with chemotherapeutic agents susceptible to redox damage. This characteristic reduces the potential for oxidative toxicity and supports its use in therapeutic regimens that minimise cellular side effects.

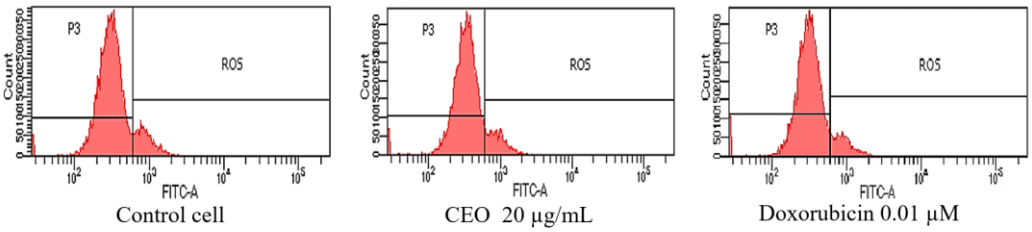

(a)

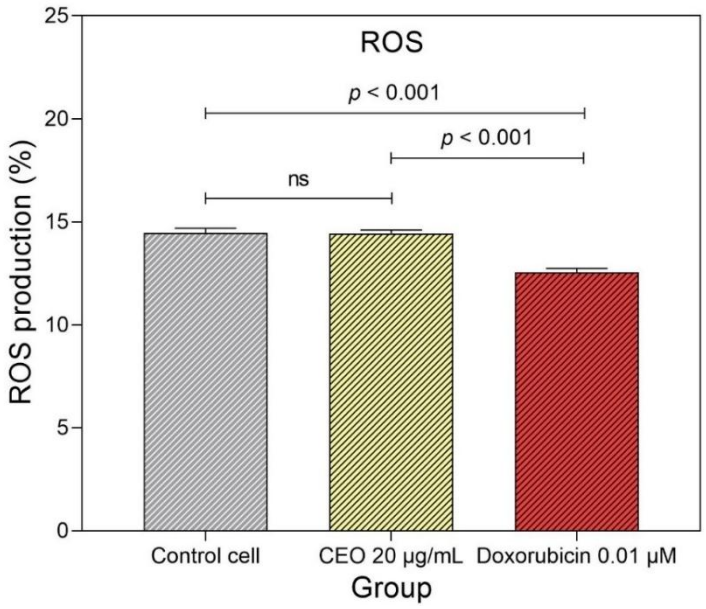

(b)

Figure 9 Intracellular ROS levels in T47D cells following 48-hour treatment with CEO (14 µg/mL) or doxorubicin (0.1 µM). (a) Representative flow cytometry histograms showing ROS fluorescence intensity. (b) Bar graph comparing ROS induction across treatment groups. $p < 0.001$ indicates statistical significance.

While the findings support the anticancer potential of *Citrus jambhiri* essential oil (CEO) through *in vitro* and network pharmacology approaches, further investigations are encouraged to strengthen translational relevance. *In vivo* studies may provide deeper insights into its pharmacokinetics and systemic effects, while additional molecular analyses could help clarify downstream signalling mechanisms. Variations in

essential oil composition due to environmental factors also present opportunities for standardisation in future research. Moreover, nanoformulation strategies, such as SLN or PLGA-based carriers, may enhance CEO's bioavailability and tumour-targeting efficiency. These approaches should be explored alongside xenograft-based *in vivo* models to validate efficacy and safety.

Conclusions

The *in vitro* and *in silico* findings collectively demonstrate that *Citrus jambhiri* essential oil (CEO) exerts selective anticancer activity against T47D breast cancer cells through a non-oxidative, multitarget mechanism. GC-MS profiling identified a predominance of monoterpenes such as D-limonene, γ-terpinene, β-pinene, α-pinene, and β-myrcene which possess physicochemical properties that promote preferential accumulation in cholesterol-rich cancer cell membranes and facilitate inhibition of the PI3K/Akt/mTOR-BTK signalling axis. Network pharmacology analysis revealed 406 compound-associated gene targets involved in cell survival pathways, while protein expression assays confirmed the downregulation of PI3K, mTOR, and BTK, with minimal impact on Akt activity preserving signalling essential for normal cell homeostasis. Biologically, CEO exhibited moderate cytotoxicity (IC_{50} = 68 µg/mL) but demonstrated a high selectivity index (SI = 4.67), inducing S-phase cell cycle arrest and apoptosis without increasing ROS levels. Compared to doxorubicin, CEO induced less necrosis and maintained ROS neutrality, underscoring its potential to reduce off-target toxicity. These findings highlight CEO's promise as an adjuvant agent capable of supporting anthracycline dose reduction to mitigate systemic toxicity. Further studies involving nanoformulation strategies and *in vivo* xenograft models are warranted to evaluate the pharmacodynamics of PI3K-BTK inhibition and to explore synergy with low-dose chemotherapy regimens. In summary, CEO selectively inhibits key oncogenic pathways PI3K/Akt/mTOR and BTK while sparing normal cells, offering a strong rationale for its development as a complementary agent in breast cancer therapy.

Acknowledgements

The author appreciated the support of the Indonesian Education Fund Management Agency and the Universitas Sumatera Utara, Indonesia for the equity funding 2023 research grant (No: 01/UN5.2.3.1/PPM/KPEP/2023, 29 December 2023).

Declaration of Generative AI in Scientific Writing

The authors acknowledge the use of generative AI tools (e.g., QuillBot and ChatGPT by OpenAI) in the preparation of this manuscript, specifically for language editing and grammar correction. No content generation or data interpretation was performed by AI. The authors take full responsibility for the content and conclusions of this work.

CRediT author statement

Fauzul Husna: Data Curation, Formal analysis, Investigation. **Poppy Anjelisa Zaitun Hasibuan:** Conceptualization, Methodology, Supervision. **Panal Sitorus:** Funding acquisition, Project administration. **Denny Satria:** Resources, Software, Validation. **Syukur Berkat Waruwu:** Writing - Original Draft, Writing - Review & Editing, Visualization. **Ema Damayanti:** Formal analysis, Resources. **Najihah Binti Hashim:** Supervision, Validation.

References

[1] IA Al Khalily, S Megantara and DL Aulifa. Targeting molecular pathways in breast cancer using plant-derived bioactive compounds: A comprehensive review. *Journal of Experimental Pharmacology* 2025; **17**, 375-401.

[2] H Sung, J Ferlay, RL Siegel, M Laversanne, I Soerjomataram, A Jemal and F Bray. Global cancer statistics 2022: GLOBOCAN estimates of incidence and mortality worldwide for 36 cancers in 185 countries. *CA: A Cancer Journal for Clinicians* 2024; **74(3)**, 229-263.

[3] J Wang and SG Wu. Breast cancer: An overview of current therapeutic strategies, challenges and perspectives. *Breast Cancer: Targets and Therapy* 2023; **15**, 721-730.

[4] A Zafar, S Khatoon, MJ Khan, J Abu and A Naeem. Advancements and limitations in traditional anticancer therapies: A csomprehensive review of surgery, chemotherapy, radiation

therapy and hormonal therapy. *Discover Oncology* 2025; **16(1)**, 607.

[5] PF Lainetti, AF Leis-Filho, R Laufer-Amorim, A Battazza and CE Fonseca-Alves. Mechanisms of resistance to chemotherapy in breast cancer and possible targets in drug delivery systems. *Pharmaceutics* 2020; **12(12)**, 1193.

[6] FM Abdoul-Latif, A Ainane, IH Aboubaker, J Mohamed and T Ainane. Exploring the potent anticancer activity of essential oils and their bioactive compounds: Mechanisms and prospects for future cancer therapy. *Pharmaceuticals* 2023; **16**, 1086.

[7] DPD Sousa, ROS Damasceno, R Amorati, HA Elshabrawy, RDD Castro, DP Bezerra, VRV Nunes, RC Gomes and TC Lima. Essential oils: Chemistry and pharmacological activities. *Biomolecules* 2023; **13**, 1144.

[8] Y Li, S Liu, C Zhao, Z Zhang, D Nie and Y Li. The chemical composition and antibacterial and antioxidant activities of 5 citrus essential oils. *Molecules* 2022; **27(20)**, 7044.

[9] K Rakoczy, N Szymańska, J Stecko, M Kisiel, M Maruszak, M Niedziela and J Kulbacka. Applications of limonene in neoplasms and non-neoplastic diseases. *International Journal of Molecular Sciences* 2025; **26**, 6359.

[10] TQ Machado, ACCD Fonseca, ABS Duarte, BK Robbs and DPD Sousa. A narrative review of the antitumor activity of monoterpenes from essential oils: An update. *BioMed Research International* 2022; **2022**, 6317201.

[11] Z Bai, C Yao, J Zhu, Y Xie, XY Ye, R Bai and T Xie. Anti-tumor drug discovery based on natural product β-elemene: Anti-tumor mechanisms and structural modification. *Molecules* 2021; **26(6)**, 1499.

[12] Yuandani, S Damayanti, D Satria, SB Waruwu and EDL Putra. Immunostimulant effects of VCO-extract of curcuminoids from turmeric rhizome (*Curcuma domestica* Val.) in cyclophosphamide and *S. aureus* infected-immunocomprised rats. *South African Journal of Botany* 2025; **184**, 399-406.

[13] K Petrotos, I Giavasis, K Gerasopoulos, C Mitsagga, C Papaioannou and P Gkoutsidis. Optimization of vacuum-microwave-assisted extraction of natural polyphenols and flavonoids from raw solid waste of the orange-juice industry at industrial scale. *Molecules* 2021; **26(1)**, 246.

[14] NA Siregar, EDL Putra, SM Sinaga, D Satria and SB Waruwu. Green synthesis of silver nanoparticles using extract of Kluwih leaves (*Artocarpus camansi* Blanco.) by microwave-assisted irradiation and their antibacterial properties. *Indonesian Journal of Applied Research* 2024; **5(3)**, 164-175.

[15] AA Amar, EDL Putra, D Satria, P Sitorus, HL Lee, SB Waruwu, M Muhammad. Biosynthesis and biological activity of silver nanoparticles from Zanthoxylum acanthopodium fruits. *South African Journal of Chemical Engineering* 2025; **52**, 271-281.

[16] A Dalimunthe, D Satria, P Sitorus, U Harahap, IFD Angela and SB Waruwu. Cardioprotective effect of hydroalcohol extract of andaliman (*Zanthoxylum acanthopodium* DC.) fruits on doxorubicin-induced rats. *Pharmaceuticals* 2024; **17(3)**, 359.

[17] M Chatri, PA Hasibuan, E Meiyanto, DP Putra, EP Septisetyani, D Satria and SB Waruwu. Effect of African leaves (*Vernonia amygdalina* Delile) on the development of T47D breast cancer cells. *Tropical Journal of Natural Product Research* 2024; **8(7)**, 7740.

[18] MJ Rodriguez, MC Perrone, M Riggio, M Palafox, V Salinas, A Elia, ND Salgueiro, AE Werbach, MP Marks, MA Kauffman, L Vellón, V Serra and V Novaro. Targeting mTOR to overcome resistance to hormone and CDK4/6 inhibitors in ER-positive breast cancer models. *Scientific Reports* 2023; **13(1)**, 2710.

[19] D Prasad, E Baldelli, EM Blais, J Davis, E El Gazzah, C Mueller, A Gomeiz, A Ibrahim, AV Newrekar, BA Corgiat, R Dunetz, IEF Petricoin, Q Wei and M Pierobon. Functional activation of the AKT-mTOR signalling axis in a real-world metastatic breast cancer cohort. *British Journal of Cancer* 2024; **131(9)**, 1543-1554.

[20] W Zhang, D Liu, X Fu, C Xiong and Q Nie. Peel essential-oil composition and antibacterial activities of Citrus×sinensis 'Tarocco' and Citrus reticulata Blanco. *Horticulturae* 2022; **8**, 793

[21] Y Wang, R Zhang, J Ma, Y Liu and J Gao. Network pharmacology-based prediction of active ingredients and mechanisms of essential oils against breast cancer. *Frontiers in Pharmacology* 2022; **13**, 908654.

[22] H Hu, H Wang, X Yang, Z Li, W Zhan, H Zhu and T Zhang. Network pharmacology analysis reveals potential targets and mechanisms of proton-pump inhibitors in breast cancer with diabetes. *Scientific Reports* 2023; **13**, 7623.

[23] D Szklarczyk, AL Gable, KC Nastou, D Lyon, R Kirsch, S Pyysalo, N Türei, TN Doncheva, M Legeay, T Fang, P Bork, LJ Jensen and CV Mering. The STRING database 2021: Customizable protein-protein networks and functional characterization of user-uploaded gene sets. *Nucleic Acids Research* 2021; **49**, D605-D612.

[24] MK Elbashir, M Mohammed, H Mwambi and B Omolo. Identification of hub genes associated with breast cancer using integrated gene-expression data with protein-protein interaction network. *Applied Sciences* 2023; **13**, 2403.

[25] BT Sherman, M Hao, J Qiu, X Jiao, MW Baseler, HC Lane, T Imamichi and W Chang. DAVID 2021 update: A web server for functional enrichment analysis and functional annotation of gene lists. *Nucleic Acids Research* 2022; **50**, W216-W221.

[26] F Karami, M Osanloo, H Alipanah, E Zarenezhad, F Moghimi and A Ghanbariasad. Comparison of the efficacy of alginate nanoparticles containing *Cymbopogon citratus* essential oil and citral on melanoma and breast-cancer cell lines under normoxic and hypoxic conditions. *BMC Complementary Medicine and Therapies* 2024; **24(1)**, 372.

[27] PAZ Hasibuan, D Satria, ER Wikantyasning, RM Harahap and M Zarlinda. Induction of apoptosis and cell-cycle arrest by *Syzygium polyanthum* extract in T47D breast-cancer cells. *Journal of Applied Pharmaceutical Science* 2022; **12**, 106-113.

[28] D Satria, PAZ Hasibuan, M Muhammad, SB Waruwu, RY Utomo and SH Ghoran. Cytotoxic and apoptotic effect of Vernonia amygdalina Delile. fractions against Hs578t triple-negative breast cancer cell lines. *Phytomedicine Plus* 2024; **4(4)**, 100640.

[29] NP Hapsari, DR Rahmawati, N Nugraheni, M Hanifa, D Satria, PAZ Hasibuan and E Meiyanto. Africa leaf (*Vernonia amygdalina* Delille.) DCM extract synergistically supports growth suppression effect of doxorubicin on MCF7 and MCF7/HER2 with different effects on cell cycle progression and apoptosis evidence. *Journal of Applied Pharmaceutical Science* 2024; **14(7)**, 075-081.

[30] DR Rahmawati, N Nugraheni, NP Hapsari, M Hanifa, RF Kastian, PW Prasetyaningrum, D Satria, PAZ Hasibuan, EP Septisetyani and E Meiyanto. Dichloromethane fraction of *Vernonia amygdalina* Delile synergistically enhances cytotoxicity of doxorubicin on 4T1 triple negative breast cancer cells through apoptosis induction and cell cycle modulation. *Indonesian Journal of Pharmacy* 2025; **36(2)**, 216-224.

[31] J Ma, C Dong, YZ Cao and BL Ma. Dual target of EGFR and mTOR suppresses triple-negative breast-cancer cell growth by regulating the phosphorylation of mTOR downstream proteins. *Breast Cancer: Targets and Therapy* 2023; **15**, 11-24.

[32] H Dostálová, R Jorda, E Řezníčková and V Kryštof. Anticancer effect of Zanubrutinib in HER2-positive breast cancer cell lines. *Investigational New Drugs* 2023; **41(2)**, 210-219.

[33] PAZ Hasibuan, RKUAB Sitorus, A Hermawan, F Huda, SB Waruwu, D Satria. Anticancer activity of the ethylacetate fraction of Vernonia amygdalina Delile towards overexpression of HER-2 breast cancer cell lines. *Pharmacia* 2024; **71**, 1–8.

[34] JM Kim, J Park, EM Noh, HK Song, SY Kang, SH Jung, JS Kim, BH Park, YR Lee and HJ Youn. Bruton's agammaglobulinemia tyrosine kinase (Btk) regulates TPA-induced breast-cancer cell invasion via PLCγ2/PKCβ/NF-κB/AP-1-dependent matrix metalloproteinase-9 activation. *Oncology Reports* 2021; **45(5)**, 56.

[35] D Mandal, P Patel, S K Verma, B R Sahu and T Parija. Proximal discrepancy in intrinsic atomic interaction arrests G2/M phase by inhibiting Cyclin B1/CDK1 to infer molecular and cellular

biocompatibility of d-limonene. *Scientific Reports* 2022; **12(1)**, 18184.

[36] J Sun, P Sun, C Kang, L Zhang, L Guo and Y Kou. Chemical composition and biological activities of essential oils from 6 Lamiaceae folk medicinal plants. *Frontiers in Plant Science* 2022; **13**, 919294.

[37] P Agarwal, Z Sebghatollahi, M Kamal, A Dhyani, A Shrivastava, KK Singh, M Sinha, N Mahato, A K Mishra and KH Baek. Citrus essential oils in aromatherapy: Therapeutic effects and mechanisms. *Antioxidants* 2022; **11**, 2374.

[38] S Nayak, RB Hegde, AS Rao and R Poojary. Unlocking the potential of essential oils in aromatic plants: A guide to recovery, modern innovations, regulation and AI integration. *Planta* 2025; **262(1)**, 6.

[39] MD Esclapez, JV García-Pérez, A Mulet and JA Cárcel. Ultrasound-assisted extraction of natural products. *Food Engineering Reviews* 2020; **3(2)**, 108-120.

[40] TN dongwe, BA Witika, NP Mncwangi, MS Poka, PP Skosana, PH Demana, B Summers and XS Noundou. Iridoid derivatives as anticancer agents: An updated review from 1970-2022. *Cancers* 2023; **15**, 770.

[41] W Saengha, T Karirat, B Buranrat, T Katisart, NL Ma and V Luang-In. Cytotoxicity and antiproliferative activity of essential oils from lemon, wild orange and petitgrain against MCF-7, HepG2 and HeLa cancer cells. *Notulae Botanicae Horti Agrobotanici Cluj-Napoca* 2022; **50(3)**, 12713.

[42] RE Kased and DME Kersh. GC-MS profiling of naturally extracted essential oils: Antimicrobial and beverage preservative actions. *Life* 2022; **12**, 1587.

[43] D Mandal, P Patel, SK Verma, BR Sahu and T Par ija. Proximal discrepancy in intrinsic atomic interaction arrests G2/M phase by inhibiting Cyclin B1/CDK1 to infer molecular and cellular biocompatibility of d-limonene. *Scientific Reports* 2022; **12(1)**, 18184.

[44] NM Alotaibi, MO Alotaibi, N Alshammari, M Adnan and M Patel. Network pharmacology combined with molecular docking, molecular dynamics, and *in vitro* experimental validation reveals the therapeutic potential of *Thymus vulgaris* L. essential oil (thyme oil) against human breast cancer. *ACS Omega* 2023; **8**, 48344-48359.

[45] M Li, J Zhang, X Chen, J Zhang and Z Chen. Screening and identification of core genes and key pathways in breast cancer using bioinformatics analysis. *Journal of Oncology* 2021; **2021**, 8434035.

[46] B Salehi, S Upadhyay, IE Orhan, AK Jugran, SLD Jayaweera, DA Dias, F Sharopov, Y Taheri, N Martins, N Baghalpour, WC Cho and J Sharifi-Rad. Therapeutic potential of α- and β-Pinene: A miracle gift of nature. *Biomolecules* 2019; **9(11)**, 738.

[47] S Yu, C Wang, J Ouyang, T Luo, F Zeng, Y Zhang, L Gao, S Huang and X Wang. Identification of candidate biomarkers correlated with the pathogenesis of breast cancer patients. *Scientific Reports* 2025; **15(1)**, 8770.

[48] W Hu, D Xu and N Li. Research status of systemic adjuvant therapy for early breast cancer. *Cancer Control* 2023; **30**, 10732748231209193.

[49] A Golestan, A Tahmasebi, N Maghsoodi, SN Faraji, C Irajie and A Ramezani. Unveiling promising breast cancer biomarkers: An integrative approach combining bioinformatics analysis and experimental verification. *BMC Cancer* 2024; **24(1)**, 155.

[50] FM Uckun and T Venkatachalam. Targeting solid tumors with Bruton's tyrosine kinase inhibitors. *Frontiers in Cell and Developmental Biology* 2021; **9**, 650414.

[51] G Maitisha, J Zhou, Y Zhao, S Han, Y Zhao, A Abliz and G Liu. Network pharmacology-based approach to investigate the molecular targets of essential oil obtained from lavender for treating breast cancer. *Heliyon* 2023; **9(11)**, e21759.

[52] K Grabowska, A Galanty, L Pecio, A Stojakowska, J Malarz, P Zmudzki, P Zagrodzki and I Podolak. Selectivity screening and structure-cytotoxic activity observations of selected oleanolic acid (OA)-type saponins from the Amaranthaceae family on a wide panel of human cancer cell lines. *Molecules* 2024; **29(16)**, 3794.

[53] S Sanshita, N Devi, B Bhattacharya, A Sharma, I Singh, P Kumar, K Huanbutta and T Sangnim. From citrus to clinic: Limonene's journey through

preclinical research, clinical trials, and formulation innovations. *International Journal of Nanomedicine* 2025; **20**, 4433-4460.

[54] AR Terry and N Hay. Emerging targets in lipid metabolism for cancer therapy. *Trends in Pharmacological Sciences* 2024; **45(6)**, 537-551.

[55] RS Ezzat, A Abdel-Moneim, KMA Zoheir, EE Mohamed, HS Abou-Seif, M Hefnawy and OM Ahmed. Anti-carcinogenic effects and mechanisms of actions of Citrus limon fruit peel hydroethanolic extract and limonene in diethylnitrosamine/2-acetylaminofluorene-induced hepatocellular carcinoma in Wistar rats. *American Journal of Cancer Research* 2024; **14**, 5193-5215.

[56] J Adamczyk-Grochala, D Bloniarz, K Zielinska, A Lewinska and M Wnuk. DNMT2/TRDMT1 gene knockout compromises doxorubicin-induced unfolded protein response and sensitizes cancer cells to ER stress-induced apoptosis. *Apoptosis* 2023; **28(1)**, 166-185.

[57] GE Lombardo, C Russo, A Maugeri and M Navarra. Sirtuins as players in the signal transduction of Citrus flavonoids. *International Journal of Molecular Sciences* 2024; **25(4)**, 1956.

[58] SA Mir, A Dar, SA Alshehri, S Wahab, L Hamid, MAA Almoyad, T Ali and GN Bader. Exploring the mTOR signalling pathway and its inhibitory scope in cancer. *Pharmaceuticals* 2023; **16(7)**, 1004.

[59] X Wu, Y Xu, Q Liang, X Yang, J Huang, J Wang, H Zhang and J Shi. Recent advances in dual PI3K/mTOR inhibitors for tumour treatment. *Frontiers in Pharmacology* 2022; **13**, 875372.

[60] Z Zuo, Z Zhou, Y Chang, Y Liu, Y Shen, Q Li and L Zhang. Ribonucleotide reductase M2 (RRM2): Regulation, function and targeting strategy in human cancer. *Genes & Diseases* 2024; **11(1)**, 218-233.

[61] F Bellanti, ARD Coda, MI Trecca, A Lo Buglio, G Serviddio and G Vendemiale. Redox imbalance in inflammation: The interplay of oxidative and reductive stress. *Antioxidants* 2025; **14(6)**, 656.

[62] R Wang, J Shang and X Zhao. Alpha-pinene induces apoptosis through oxidative stress and PI3K/AKT/NF-κB signalling pathway in MDA-MB-231 human breast cancer cells. *International Journal of Pharmacology* 2021; **17(6)**, 391-399.

[63] X Zhang, R Gao, Z Zhou, X Tang, J Lin, L Wang, X Zhou and T Shen. A network pharmacology-based approach for predicting active ingredients and potential mechanism of Lianhuaqingwen capsule in treating COVID-19. *International Journal of Medical Sciences* 2021; **18(8)**, 1866-1876.

[64] FM Abdoul-Latif, A Ainane, IH Aboubaker, J Mohamed and T Ainane. Exploring the potent anticancer activity of essential oils and their bioactive compounds: Mechanisms and prospects for future cancer therapy. *Pharmaceuticals* 2023; **16(8)**, 1086.

[65] N Gautam, AK Mantha and S Mittal. Essential oils and their constituents as anticancer agents: A mechanistic view. *BioMed Research International* 2014; **2014(1)**, 154106.

[66] A Terasaki, H Kurokawa, H Ito, Y Komatsu, D Matano, M Terasaki, H Bando, H Hara and H Matsui. Elevated production of mitochondrial reactive oxygen species via hyperthermia enhanced cytotoxic effect of doxorubicin in human breast cancer cell lines MDA-MB-453 and MCF-7. *International Journal of Molecular Sciences* 2020; **21(24)**, 9522.

[67] P Wigner, K Zielinski, M Labieniec-Watala, A Marczak and M Szwed. Doxorubicin-transferrin conjugate alters mitochondrial homeostasis and energy metabolism in human breast cancer cells. *Scientific Reports* 2021; **11(1)**, 4544.